ACS OMEGA

Open Access

http://pubs.acs.org/journal/acsodf

Article

Simulation of a Multistaggered Baffle Scrubber to Enhance the Efficiency of Simultaneous Desulfurization and Denitrification

Yijie Zeng, Byoung-Hwa Lee, Kang-Min Kim, Min-Woo Kim, Young-Joo Lee, Young-Chan Choi, Jong Won Choi, and Chung-Hwan Jeon*

Cite This: *ACS Omega* 2024, 9, 15372−15382

Read Online

ACCESS | Metrics & More | Article Recommendations

ABSTRACT: In this study, we conduct simulation research on simultaneous desulfurization and denitrification in a multistaggered baffle spray scrubber. By employing two-phase flow simulations within the Euler−Lagrange framework and calculating the gas−liquid mass transfer rate with user-defined functions, we comprehensively analyzed the effects of various operational parameters. Initially, we validated our simulation model by comparing the simulation results with experimental data. Under conditions of a 0.2 mm droplet diameter, a liquid-to-gas ratio (L/G) of 12 L/m^3, and a gas flow rate of 5 CMM using a full cone nozzle, the simulation indicated a desulfurization efficiency of 99.90 versus 99.84% obtained experimentally and a denitrification efficiency of 92.01 versus 90.67% obtained experimentally. This comparison confirmed the reliability of the simulation model. Our findings indicate that a droplet size of 2 mm is optimal, enhancing the desulfurization efficiency from 99.90 to 99.98% and the denitrification efficiency from 92.01 to 99.76%. However, when the droplet size exceeds 2 mm, efficiencies marginally decrease. Increasing the liquid-to-gas ratio to 16 L/m^3 further improves desulfurization and denitrification efficiencies to 99.98 and 99.80%, respectively. In contrast, higher inlet flue gas flow rates reduce these efficiencies, with a decline observed from 100% to as low as 93.90% for denitrification with 2 mm droplets. Additionally, the use of a swirl cone nozzle, compared to full or hollow cone nozzles, better disperses droplets, enhancing the gas−liquid contact and achieving efficiencies of 99.99% for desulfurization and 99.81% for denitrification with 2 mm droplets. These insights are valuable for optimizing operational conditions in industrial-scale spray scrubbers, significantly contributing to mitigating the environmental impacts of industrial emissions.

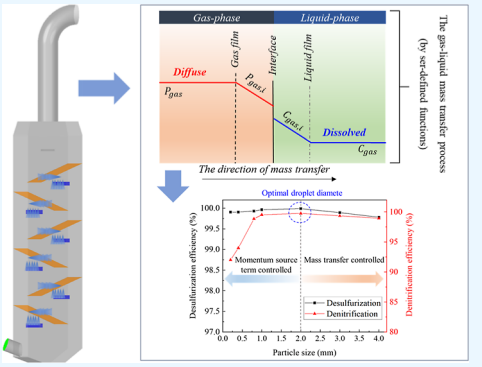

1. INTRODUCTION

SO_2 and NO emissions are important contributors to air pollution. These emissions have negative effects on human health, particularly on the respiratory system.[1−3] Furthermore, SO_2 and NO are responsible for acid rain and ozone depletion.[4] Increased environmental consciousness and worldwide sustainable development have led to increasingly strict industrial emission requirements. Currently, the methods widely utilized in the industrial emission treatment include the optimized combustion technology,[5,6] selective catalytic reduction (SCR),[7,8] adsorption,[9] absorption,[10−12] and electron beam technology.[13,14] However, each of these methods has limitations owing to the various requirements for gas management under different industrial settings, operating conditions, and running costs.[11]

SCR is a posttreatment method for the efficient control of NO emission.[8] It cannot be used to control SO_2 in exhaust gas; therefore, large industrial facilities usually employ combined SCR and flue gas desulfurization (FGD) systems to achieve simultaneous sulfur and nitrogen removal. Additionally, activated carbon is another option, capable of adsorbing SO_2 and NO with high efficiency from exhaust gases. However, the efficiency of the material decreases during continuous absorption, and treating exhaust gases from large industrial facilities is impossible.[15] Compared with other technologies, traditional wet scrubbing techniques are less efficient and require a scrubbing solution, which is considered a secondary pollutant. However, the simplicity of such techniques with regard to the structure and operating environment renders them suitable for high-flow exhaust gases and capable of simultaneously treating NO, SO_2, and particulate matter in exhaust gases.[16−19]

Qu et al. simulated the wet flue gas desulfurization (WFGD) scrubber system of a 330 MW coal-fired unit to increase its operating efficiency through optimization.[17] Their findings

Received: December 21, 2023
Revised: January 28, 2024
Accepted: February 29, 2024
Published: March 18, 2024

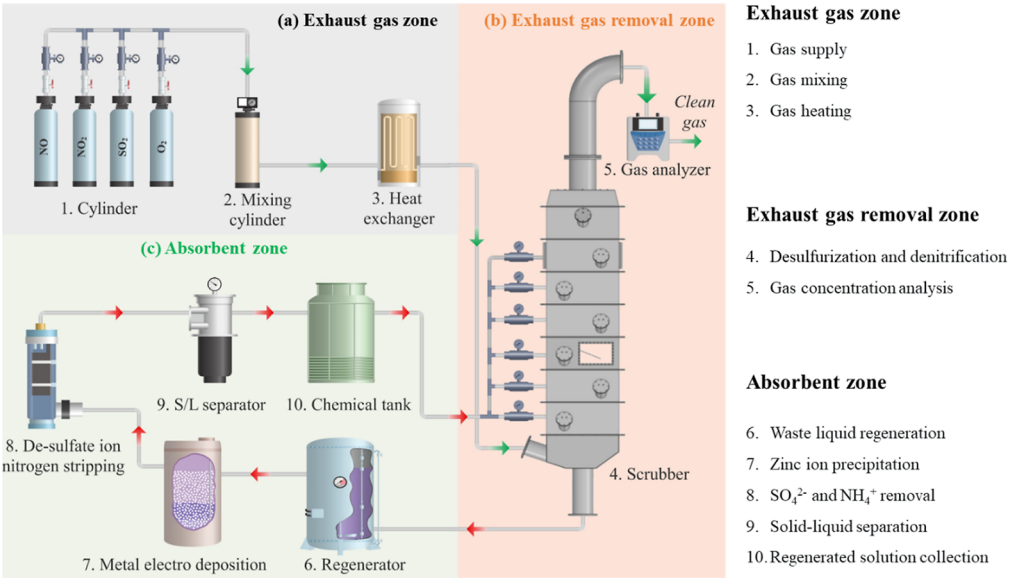

Figure 1. Schematic of the experimental setup of the multistaggered baffle spray scrubber system (green and red arrows indicate the directions of gas and solution movement, respectively).

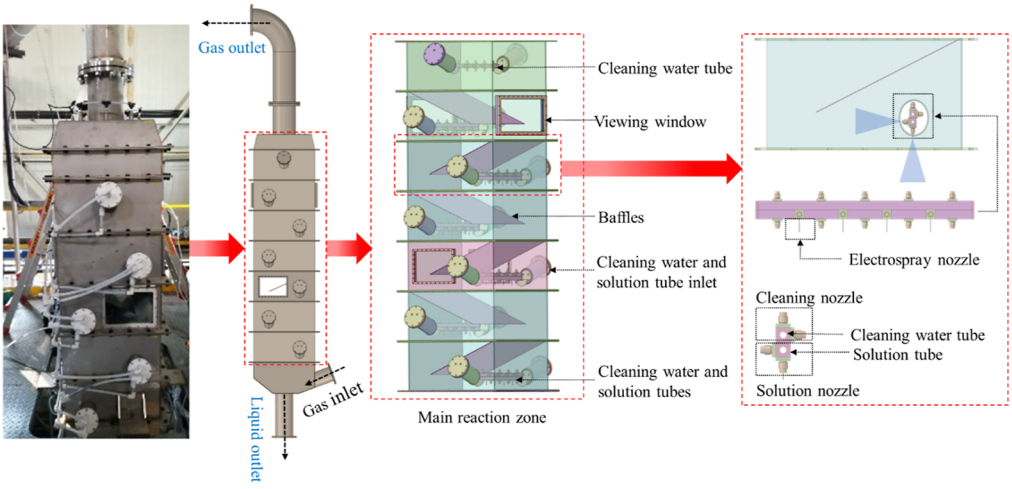

Figure 2. Schematic of the multistaggered baffle spray scrubber and the layout of each stage.

indicated that compared with single-direction injection, dual-direction injection was advantageous for achieving a uniform flow and enhancing mass transfer. Additionally, the authors compared the ideal plug flow with a nonideal flow and found that under the ideal plug flow, the desulfurization efficiency increased with a reduction in the spray droplet size. In contrast, under the nonideal flow, an optimal droplet size was observed. They also proposed a design layout that combined full and hollow cones to increase the overall desulfurization efficiency of the unit. Droplets played an essential role in the flue gas absorption process, and changing the droplet diameter, nozzle type, and injection direction, among other methods, was both efficient and cost-effective. However, most studies have focused on vertical injection with limited exploration of lateral nozzles. And studies on the alteration of the nozzle swirl fraction are lacking. Another method for enhancing mass transfer is to optimize the internal structure of the scrubber. Chen et al. established a pilot-scale experimental facility to evaluate the WFGD of a 600 MW coal-fired power plant at a 1:15 scale.[18] The authors added baffle plates to avoid local high-speed flow and enhance gas−liquid interactions. Kurella and Meikap found that a multistage dual-flow screen plate scrubber was advantageous for increasing the contact time and interface area between the gas and liquid phases.[21,22] Tran et al. conducted laboratory-scale experiments on a simulated wet scrubber-based filtered containment venting system and found that the baffles blocked the upward flow of gas, increased the gas residence time, and suppressed the entrainment of liquid droplets from the spray scrubber.[23] Diversion plates, screen plates, and baffles not only serve as flow directors but also effectively extend the flue gas residence time, enhancing gas−liquid interactions.[24,25] However, research on baffle-type spray scrubbers is lacking.

In this study, a novel multistaggered baffle spray scrubber was developed, which enhances the residence time of flue gases through the use of baffles and broadens the spray coverage by employing both lateral and longitudinal bidirectional spraying to enhance gas−liquid contact. This study represents the first attempt to simulate the absorption of SO_2 and NO by Fe(II)(EDTA) solution droplets using user-defined function

https://doi.org/10.1021/acsomega.3c10223
ACS Omega 2024, 9, 15372−15382

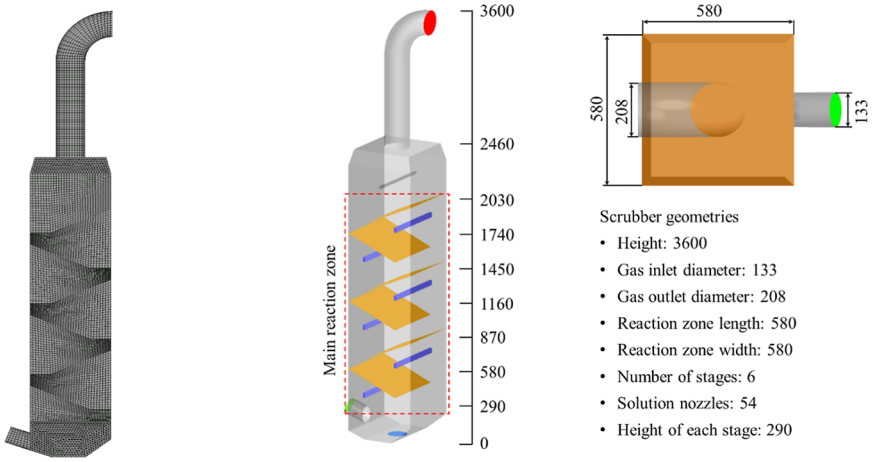

(a) Meshing of the computational domain (b) Computational domain (c) Top view of the scrubber

Figure 3. Geometries for simulation and data selection (unit: mm).

(UDF) codes within the framework of the Euler−Lagrange computational fluid dynamics model. We also investigated the effects of particle size, liquid-to-gas (L/G) ratio, inlet gas flow rate, and nozzle type on the efficiencies of simultaneous desulfurization and denitrification. The findings provide valuable guidance for the scale-up and design of wet scrubbers.

2. EXPERIMENTAL SECTION

2.1. Experimental Procedure. Figure 1 shows the experimental system used for simultaneous wet desulfurization and denitrification. The experimental setup consisted of three main parts. First, in the exhaust gas zone (a), the mixed experimental gases flowed into the heat exchanger for temperature adjustment. Subsequently, in exhaust gas removal zone (b), SO_2 and NO were introduced into the scrubber for capture. Subsequently, the purified gas was expelled from the gas outlet, and the gas concentration was measured using a gas analyzer (testo 350 K). The washing solution containing Fe(II)(EDTA)-NO was discharged from the lower part of the scrubber and entered the absorbent zone (c). Finally, the solution was recycled into the spray scrubber through continuous filtration for reuse.

2.2. System Description. Figure 2 presents the working principle and internal structure of a multistaggered baffle spray scrubber. Polluted flue gas first enters from the bottom inlet of the desulfurization scrubber and then flows upward along the baffles. During the ascent, the flue gas encounters liquid droplets sprayed from nozzles, coming into contact with them in the reaction zone and undergoing purification. The cleaned flue gas is then discharged from the top of the scrubber, while the cleaning solution used is drained from the bottom. The key part of the scrubber is a six-segment main reaction area, with each segment consisting of baffles, cleaning water, and solution tubes. The pipes are rectangular, and each face is fitted with full cone nozzles: there are four nozzles on each horizontal face and five on each vertical face. This arrangement facilitates effective contact between the spray and flue gas. During the operation of the scrubber, the horizontal inward and vertical downward nozzles are opened. Conversely, the nozzles directed toward the wall and those oriented vertically upward are engaged exclusively when the scrubber is not operating, serving to cleanse residues within the spray tower. Figure 3 depicts the simulated computational domain, including the main reaction area and the inlet and outlet sections with the dimensions and specifications of the spray tower marked. Table 1 presents the experimental conditions on which the simulation studies were based.

Table 1. Experimental Operating Conditions

parameter	value	parameter	value
continuous phase (flue gas)		dispersed phase (slurry droplets)	
flow rate (CMM, dry basis)	2400	total flow rate (LPM)	60
inlet temperature (K)	313.15	droplet diameter distribution (μm)	200
inlet NO concentration (ppm)	300		
inlet SO_2 concentration (ppm)	699		

3. MATHEMATICAL METHODS

3.1. Assumptions. The gas- and liquid-phase flow fields of the multistaggered baffle spray scrubber were computed within the computational domain of the Euler−Lagrange framework. The simulation calculation areas are shown in Figure 3a,b. A realizable k-epsilon model was employed to calculate the turbulent viscosity. To increase the computational accuracy, hexahedral meshes were primarily used in the core reaction zone where the main chemical reactions occurred. The simulation adopted a model consisting of 502,205 elements. Given the complexity of the spray scrubber's structure, which involves intricate flow fields and the mass transfer, heat transfer, and chemical reactions between the two phases, it is highly challenging to accurately simulate all these processes. Therefore, according to the literature, the following assumptions were made to simplify the model:[17,20,26]

A. The gas phase was considered an incompressible Newtonian fluid.
B. The chemical reaction processes within the scrubber were neglected.
C. Each liquid droplet was treated as a nonrotating rigid sphere. Collisions and coalescence between the droplets and wall film were ignored.

3.2. Continuous Phase. Within the spray scrubber, the flue gas is treated as a continuous phase and is calculated

https://doi.org/10.1021/acsomega.3c10223
ACS Omega 2024, 9, 15372−15382

Table 2. Governing Equations for the Flue Gas

continuity	$\frac{\partial}{\partial t}\rho_g + \nabla\cdot(\rho_g\vec{u}_g) = S_{mass}$	(1)
momentum	$\frac{\partial}{\partial t}(\rho_g\vec{u}_g) + \nabla\cdot(\rho_g\vec{u}_g\vec{u}_g) = -\nabla p + \nabla\cdot\bar{\bar{\tau}} + \rho_g\vec{g} + S_{mom}$	(2)
energy	$\frac{\partial}{\partial t}(\rho_g e) + \nabla\cdot(\rho_g e\vec{u}_g) = -\nabla p\nabla\cdot\vec{u}_g + \nabla\cdot(k_{eff}\nabla T + \bar{\bar{\tau}}_{eff}\cdot\vec{u}_g - \sum h_k\vec{J}_k) + S_{en}$	(3)
species	$\frac{\partial}{\partial t}(\rho Y_k) + \nabla\cdot(\rho_g\vec{u}_g Y_k) = \nabla\cdot\vec{j}_k + S_{k,mass}$	(4)

according to the conservation laws of momentum, energy, and mass for the continuous phase. The governing equations for the flue gas are presented in Table 2.[19,20,27,28]

3.3. Dispersed Phase. In the Lagrangian framework, the motion of liquid droplets is calculated by using the discrete phase model. The equation describing the motion of an individual droplet is defined by eq 5, and the governing equations for the droplets are presented in Table 3.[7,17,19,29]

Table 3. Governing Equations for the Droplets

equation of motion for a single droplet	$\frac{d\vec{x}}{dt} = \vec{u}_d$	(5)
mass	$\frac{dm_d}{dt} = S_{k,mass}$	(6)
force	$m_d\frac{dv}{dt} = S_{k,mom} + m_d g$	(7)
energy	$m_d c_d\frac{dT_d}{dt} = S_{k,en}$	(8)

3.4. Two-Phase Transfer. In this study, we primarily considered the processes of SO_2 and NO absorption by a solution, neglecting water evaporation. The equations for the two-phase transfer are presented in Table 4. Consequently,

Table 4. Equations for the Two-Phase Transfer

mass source term	$S_{i,mass} = \dot{m}_{SO_2} + \dot{m}_{no}$	(9)
mass transfer rate of gas into droplets	$S_g = -J_g = -K_{g,tot}A_d(P_g - C_l/H_g)$	(10)
momentum source term	$S_{i,mom} = \frac{1}{2}\rho_g\lvert\vec{u}_g - \vec{u}_d\rvert(\vec{u}_g - \vec{u}_d)C_dA_d + m_d g$	(11)

only SO_2 and NO are present in the gas−liquid mass transfer process, and the mass source term can be represented by eq 9. The mass transfer process between the gas and liquid phases is influenced by the partial pressures of both phases. Following the dual-mode theory, the mass transfer rates of SO_2 and NO can be expressed by eq 10.[17,19,20,26,30] Considering gravity and resistance as two key forces in a two-phase flow, the momentum source term, which refers to Crowe's formulation in eq 8, can be expressed as eq 11.[20,29] Here, C_d is the drag coefficient, which depends on the Reynolds number of the liquid droplets and is calculated using the correlation established by Morsi and Alexander.[31] The mass and heat transfer processes of SO_2 and NO in the liquid phase were coupled by using UDF codes.

3.5. Chemical Reactions in the SO_2 Absorption Process. $K_{SO_2,tot}$ is the total mass transfer coefficient, which is expressed as[17,32]

$$k_{SO_2,tot} = \left[\frac{1}{K_{so_2,g}} - \frac{H_{so_2}}{E_{so_2}K_{so_2,l}}\right]^{0.5} \quad (12)$$

where $k_{SO_2,l}$ is the liquid-phase mass transfer coefficient for the physical absorption process,[17,19,20,33] which is expressed as

$$k_{SO_2,l} = 0.88\left[\left(\frac{8\sigma_{d-g}}{3\pi m_d}\right)^{0.5} D_{SO_2,l}\right]^{0.5} \quad (13)$$

and $k_{SO_2,g}$ is the gas-phase mass transfer coefficient, which is determined using the modified Ranz−Marshall equation[17,34]

$$k_{SO_2,g} = \frac{2 + 0.6\mathrm{Re}^{0.5}Sc^{0.33}D_{SO_2,g}}{d_p RT} \quad (14)$$

3.6. Chemical Reactions in the NO Absorption Process. The mass transfer coefficients in the gas and liquid phases can be calculated using eqs 15 and 16, respectively.[35,36] In these equations, $K_{CO_2,l}$ and $K_{CO_2,g}$ are the mass transfer coefficients of CO_2 in the liquid and gas phases, respectively, D_{NO-H_2O} and $D_{CO_2-H_2O}$ are the liquid diffusion coefficients of NO and CO_2 in H_2O, respectively, and D_{NO-N2} and D_{CO_2-NO} are the gas diffusion coefficients (m^2/s) of NO and CO_2 in N_2, respectively (see ref 35 for the calculation method).

$$k_{NO,l} = K_{CO_2,l}\left(\frac{D_{NO-H_2O}}{D_{CO2-H_2O}}\right)^{\lambda} \quad (15)$$

$$k_{NO,g} = K_{CO_2,g}\left(\frac{D_{NO-N_2}}{D_{CO_2-NO}}\right)^{\lambda} \quad (16)$$

4. RESULTS AND DISCUSSION

4.1. Experimental Validation of Simulation Results. The feasibility of the model was verified by comparing the experimental smoke concentrations obtained at the outlet of the spray scrubber to the simulation results. Efficiency was defined as follows

$$\eta_i = \frac{C_{i.inlet} - C_{i,outlet}}{C_{i,inlet}} \times 100\% \quad (17)$$

where η_i represents the desulfurization or denitrification efficiency, $C_{i,inlet}$ represents the inlet concentration of a gas, and $C_{i,outlet}$ represents the outlet concentration of the gas. Table 5 presents a comparison between experimental measurements and simulated values. As shown, the simulation results were similar to the experimental outcomes.

https://doi.org/10.1021/acsomega.3c10223
ACS Omega 2024, 9, 15372−15382

Table 5. Simulation and Experimental Results

	desulfurization efficiency	denitrification efficiency
experimental results (%)	99.84	90.67
simulation results (%)	99.90	92.01
error (%)[a]	0.06	1.48

[a]Error = (calculated − measured) × 100/measured.

4.2. Effect of Liquid Particle Size. In a counter-current scrubber, reducing the diameter of spray droplets can increase the gas−liquid contact area, increasing the mass transfer efficiency. However, reducing the droplet size will reduce the terminal velocity of the droplets,[16] which reduces the relative slippage speed between the gas and liquid phases, reducing the momentum source terms (eq 11).[19,37−39] Additionally, increasing the droplet diameter, although beneficial for improving the uniformity of the airflow, reduces the gas−liquid contact area, reducing the mass transfer rate (eq 10).[16,19,40,41] In fact, there is an optimal droplet diameter that maintains stable droplet motion while balancing the relationship between momentum transfer and mass transfer efficiency, thus increasing the efficiency of the scrubber.[19,41]

In this study, to further investigate the specific impact of the droplet diameter on the efficiency of the scrubber, seven different droplet sizes of 0.2, 0.4, 0.8, 1, 2, 3, and 4 mm were selected for examination. Figure 4 presents the efficiencies of desulfurization and denitrification at the outlet of the scrubber for different droplet sizes, and Figure 5 shows the variation in the desulfurization and denitrification efficiencies with different droplet sizes as the height of the scrubber increases. Within the range of 0.2−2 mm, the efficiencies of both desulfurization and denitrification increased, with the desulfurization efficiency slightly increasing from 99.90 to 99.98%. In comparison, the efficiency of denitrification increased from 92.01% at a droplet diameter of 0.2 mm to 99.76% at 2 mm, corresponding to an increase of >7%. However, as the droplet diameter increased from 2 to 4 mm, slight reductions were observed: the desulfurization efficiency decreased from 99.98 to 99.78% and the denitrification efficiency decreased from 99.76 to 98.95%. Despite these reductions, the efficiency of desulfurization remained comparatively high. Furthermore, the efficiencies of desulfurization and denitrification at various heights in the main reaction area were consistent with the final outlet results, indicating an efficiency peak at a droplet size of 2 mm.

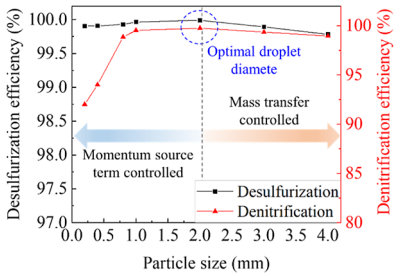

Figure 4. Simultaneous desulfurization and denitrification efficiencies of the scrubber as a function of droplet size.

Figure 6 illustrates the droplet movement trajectories, further revealing this phenomenon. Droplets with a diameter of 0.2 mm had unstable trajectories owing to airflow disturbances, leading to turbulence and collisions with the tower walls and baffles. When the diameter increased to 0.4 mm, some droplets were still affected by the airflow. However, starting from 0.8 mm, as the droplet diameter increased, the movement trajectory of the droplets gradually became more stable. Unsteady motion of droplets adversely affected the efficiencies of the desulfurization and denitrification processes.[19] However, there was no occurrence of droplets being entrained out of the spray tower, indicating that the multistaggered baffles can effectively prevent droplet entrainment, which is consistent with the findings of previous research.[23] However, as the droplet diameter continued to increase from 2 to 4 mm, the motion of the droplets stabilized. The increase in the droplet diameter reduced the gas−liquid contact area, weakening mass transfer.

For smaller droplets (with diameters ranging from 0.2 to 2 mm), the mass transfer efficiency was primarily influenced by the airflow. In this case, the droplets experienced an uneven distribution and were more susceptible to being carried along with the airflow, resulting in collisions with the walls and

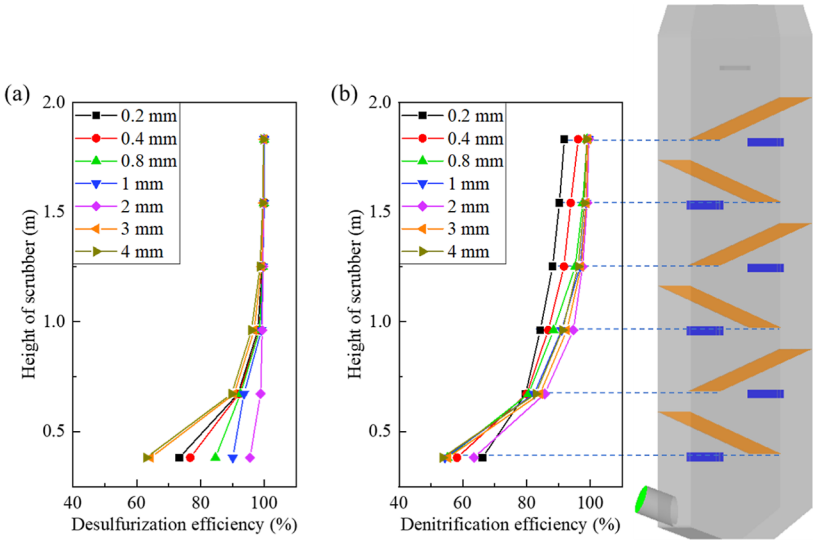

Figure 5. Simultaneous (a) desulfurization and (b) denitrification efficiencies obtained from the scrubber at different heights and droplet sizes.

https://doi.org/10.1021/acsomega.3c10223
ACS Omega 2024, 9, 15372−15382

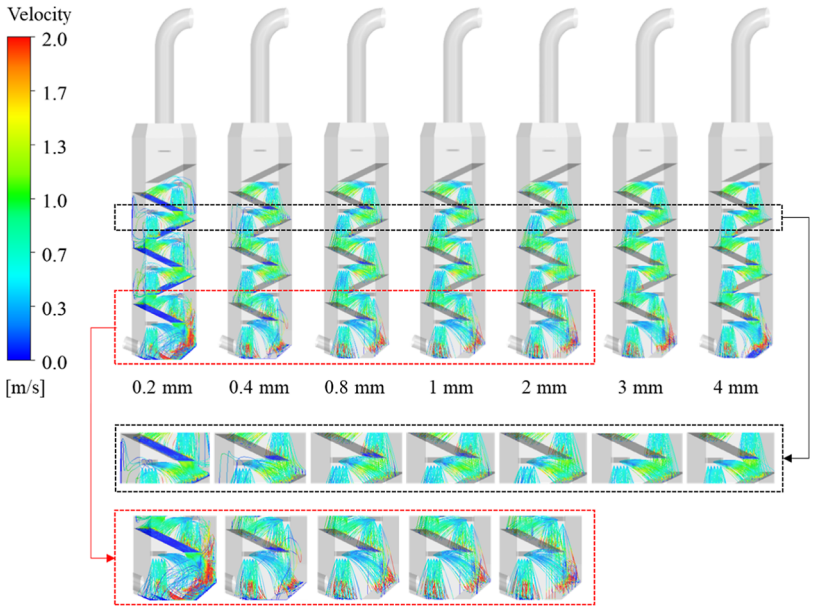

Figure 6. Trajectories of droplets with different diameters colored by velocity.

baffles and reductions in the absorption efficiency for SO_2 and NO. When the diameter of the droplets exceeded 2 mm, the desulfurization and denitrification efficiencies were predominantly influenced by the mass transfer rate; i.e., an increase in particle size reduces the effective reaction surface area, reducing the absorption efficiency of the scrubber. Therefore, the optimal droplet diameter for the spray scrubber, which can be adjusted by modifying the spray nozzles to control the droplet size, is 2 mm.

4.3. Effect of the Inlet Gas Flow Rate. Given that the flue gas emissions at the outlet of experimental and industrial equipment are not always uniform, it is important to study the effects of the flue gas flow rate on the simultaneous desulfurization and denitrification efficiencies of the scrubber.[27] The flow rate of the flue gas directly affects the absorption rate of the scrubbing liquid on the flue gas, which determines the purification efficiency of the flue gas. The effects of different flue gas flow rates on the removal rates of SO_2 and NO are shown in Figure 7. As the inlet flue gas flow

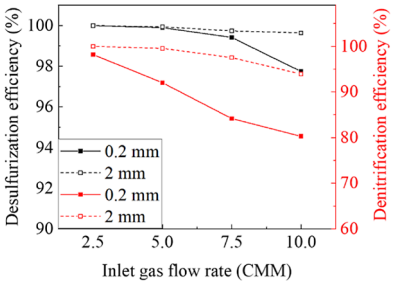

Figure 7. Simultaneous desulfurization and denitrification efficiencies of the scrubber under different inlet gas flow rates.

rate increased, the simultaneous desulfurization and denitrification efficiencies decreased from 100 to 99.64% and from 100 to 93.90%, respectively, for droplets with a diameter of 2 mm. For droplets with a diameter of 0.2 mm, the simultaneous desulfurization and denitrification efficiencies decreased from 100 to 97.74% and from 98.19 to 80.25%, respectively. When the inlet flue gas flow rate was increased, the efficiencies of desulfurization and denitrification decreased. This was due to the increased flow rate, resulting in a lower molar ratio of the flue gas to the scrubbing solution, which reduced the simultaneous removal efficiency of SO_2 and NO. Second, as indicated by the velocity streamlines shown in Figure 8a,c, an increase in the inlet flue gas flow rate accelerated the flow of the flue gas through the scrubber. This reduced the residence time of the flue gas within the scrubber, reducing the removal rates of SO_2 and NO. Moreover, the gas flow speed was higher at a droplet size of 0.2 mm than that at 2 mm. This suggests that larger droplet sizes are beneficial for slowing the gas flow, which can extend the gas−liquid contact time and consequently increase the efficiencies of desulfurization and denitrification.

Finally, an increase in the flue gas velocity disrupted the movement trajectory of the spray droplets. Figure 8b,d shows the movement trajectories of droplets with diameters of 0.2 and 2 mm, respectively. As the inlet flue gas flow rate increased from 2.5 to 10 CMM, the droplet movement trajectory became turbulent. In particular, at inlet flue gas flow rates of ≥7.5 CMM, numerous droplets collided with the walls and baffles as they flowed; some droplets were even carried out of the scrubber (when the droplet diameter was 0.2 mm). However, when the droplet diameter was 2 mm, the droplets maintained a uniform flow within the spray scrubber, even with increases in the inlet flow rate. These findings indicate that larger droplets result in a more stable flow field.

Increasing the inlet flue gas flow rate is equivalent to increasing the reactant concentration and increasing the flow velocity, both of which reduce the residence time of the flue gas within the spray scrubber and the absorption efficiencies of SO_2 and NO. They may also lead to disrupted droplet movement trajectories, adversely affecting flue gas absorption. Therefore, a low inlet flue gas flow rate is favorable for capturing SO_2 and NO. If increases in the inlet flue gas flow rate are necessary, then the use of larger droplets may be considered to mitigate the adverse effects of this parameter and maintain effective absorption.

https://doi.org/10.1021/acsomega.3c10223
ACS Omega 2024, 9, 15372−15382

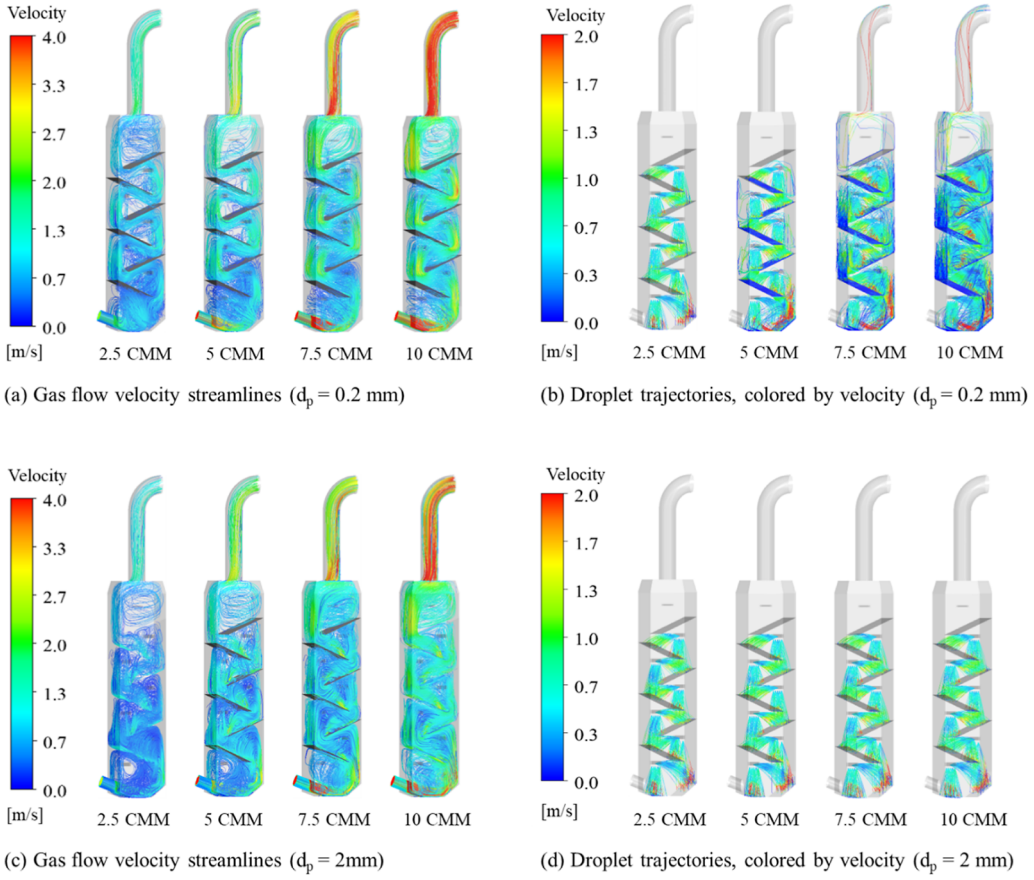

Figure 8. Gas flow velocity streamlines and droplet trajectories obtained under different gas flow rates and droplet diameters.

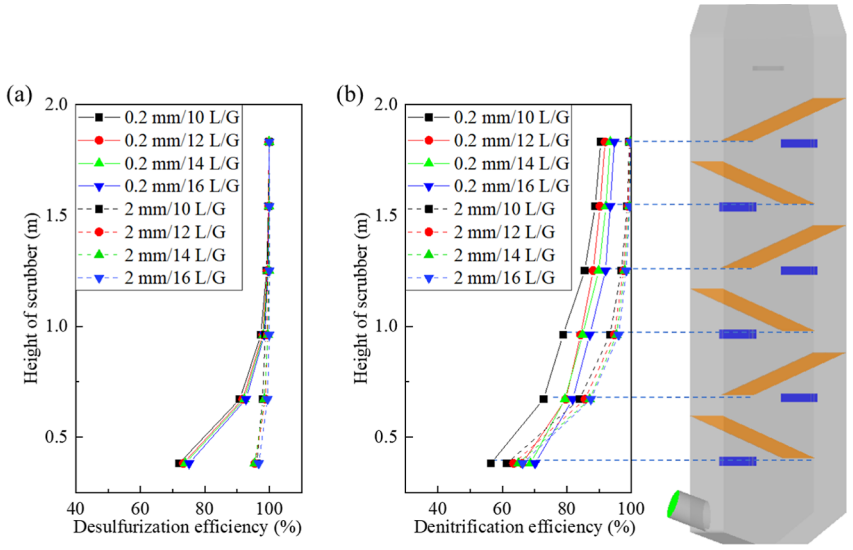

Figure 9. Simultaneous (a) desulfurization and (b) denitrification efficiencies of the scrubber at different heights and liquid-to-gas ratios.

4.4. Effect of the Liquid-To-Gas Ratio. The liquid-to-gas ratio (L/G) is one of the critical factors determining the removal efficiency of scrubbers. It is defined as the ratio of the flow rate of the scrubbing liquid (L/min) to the flow rate of the simulated exhaust gas (Nm^3/min) in the scrubber.[42] By keeping the inlet flue gas flow rate constant and adjusting the flow of the reaction liquid, the L/G ratio can be modified. Figure 9 shows the effects of different L/G ratios on the efficiencies of desulfurization and denitrification. Our results indicated that increasing the L/G ratio increased the desulfurization and denitrification efficiencies. Specifically, at an L/G ratio of 16 L/m^3 and a droplet diameter of 2 mm, the desulfurization and denitrification efficiencies reached 99.98 and 99.80%, respectively. The efficiency increased rapidly from the lower part of the scrubber to the middle part; however, as the height increased (closer to the outlet), the rate of improvement decreased. Comparing the SO_2 and NO concentration distributions in Figure 10 reveals that the

https://doi.org/10.1021/acsomega.3c10223
ACS Omega 2024, 9, 15372−15382

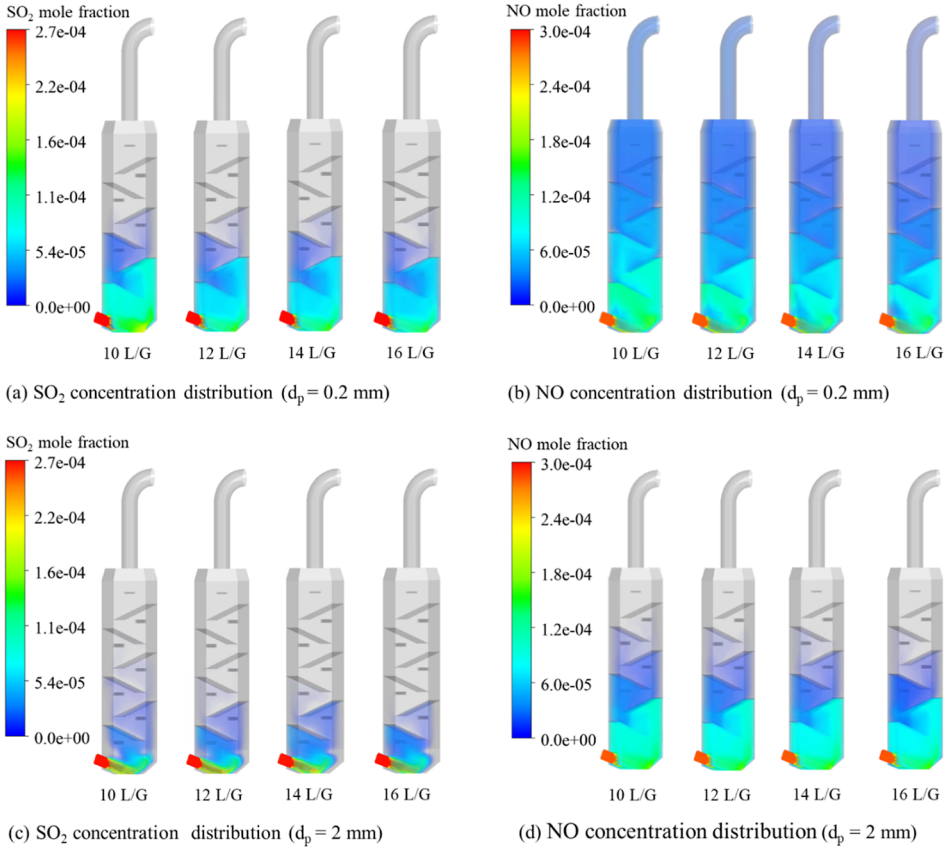

Figure 10. SO_2 and NO concentrations with different liquid-to-gas ratios and droplet diameters.

concentrations of SO_2 and NO were relatively high when the flue gas initially entered the scrubber. As the flue gas rose, it quickly encountered the reaction solution and was absorbed by it. As desulfurization and denitrification proceeded, the SO_2 and NO concentrations decreased. Increasing the L/G ratio accelerated the absorption of flue gas by the droplets. Figure 11

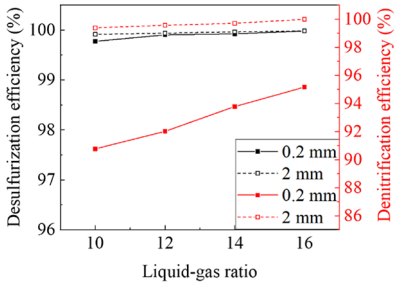

Figure 11. Simultaneous desulfurization and denitrification efficiencies of the scrubber at different liquid-to-gas ratios.

shows the efficiencies of desulfurization and denitrification at the outlet of the scrubber. Because the desulfurization efficiency was already at a high level, changing the L/G ratio had a relatively small impact on it. However, there was a significant increase in the denitrification efficiency.

Increases in the L/G ratio imply an increase in the flow rate of the scrubbing liquid, which increases the contact area between the flue gas and droplets. Although the results indicate that increasing the L/G ratio improves the desulfurization and denitrification efficiencies of the scrubber, the relative droplet diameter and inlet flue gas flow rate have a small impact on these efficiencies. However, increasing the flow rate of the scrubbing liquid increases the operating cost of the spray scrubber. Therefore, adjusting the droplet size and reducing the inlet flue gas flow rate may be cost-effective measures to improve the desulfurization and denitrification efficiencies of the scrubber while minimizing operating expenses.

4.5. Effect of the Nozzle Cone Type. In this study, we used three types of nozzles: a full cone, a hollow cone, and a swirl cone, to investigate the effects of the nozzle type on the desulfurization and denitrification efficiencies of the scrubber through simulations. Figure 12 illustrates how the different

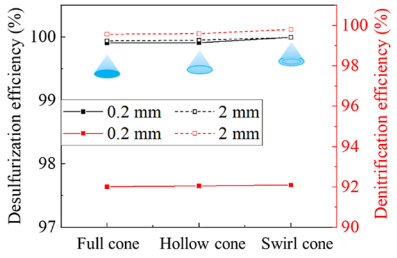

Figure 12. Simultaneous desulfurization and denitrification efficiencies of the scrubber with different nozzles.

nozzles affect these efficiencies. The results indicate that the hollow cone's efficiency was slightly higher than that of the full cone. However, this efficiency difference was not significant, suggesting that both nozzle types have similar effects on desulfurization and denitrification. In contrast, the use of the swirl cone nozzle led to an overall increase in the absorption efficiency. In particular, when the swirl cone nozzle was utilized

https://doi.org/10.1021/acsomega.3c10223
ACS Omega 2024, 9, 15372−15382

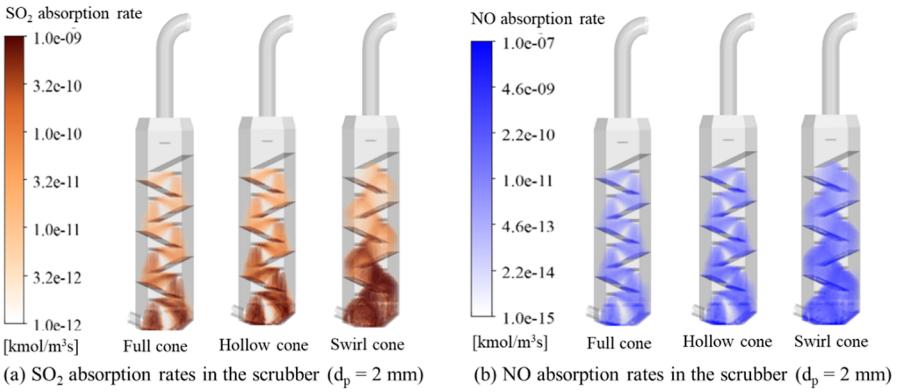

Figure 13. SO_2 and NO absorption rates in the scrubber with different nozzles.

with a droplet diameter of 2 mm, we achieved even higher simultaneous desulfurization and denitrification efficiencies: 99.99 and 99.81%, respectively. This indicates the effectiveness of the swirl cone nozzle for optimizing the scrubbing process under specific conditions. Figure 13 shows the SO_2 and NO absorption rates for the three nozzle types. The full cone and hollow cone nozzles produced similar spray patterns, but the hollow cone nozzle exhibited slightly higher absorption rates due to its better dispersion characteristics. The swirl cone nozzle, however, generated a broader spray area, enhancing the gas−liquid contact area and thus improving gas absorption. Therefore, a swirl cone nozzle is preferable for optimizing droplet absorption.

5. CONCLUSIONS

This study presents the first attempt to simulate simultaneous desulfurization and denitrification using a novel multistaggered baffle spray scrubber with an Fe(II)(EDTA) scrubbing solution. The effects of the droplet size, inlet flue gas flow rate, L/G ratio, and nozzle type on simultaneous desulfurization and denitrification were explored, and the following conclusions were drawn.

(1) The simultaneous desulfurization and denitrification efficiencies of the multistage baffle wet scrubber were influenced by the flow pattern and mass transfer, which exerted competing effects. When the droplet diameter was 2 mm, a balance between these properties was achieved, leading to optimal simultaneous desulfurization and denitrification efficiencies: 99.98% for desulfurization and 99.76% for denitrification.

(2) Increasing the inlet flue gas flow rate increases the gas velocity, leading to reductions in the residence time of the flue gas within the scrubber and potential instability in the droplet flow; in some cases, it can even lead to the entrainment of droplets out of the scrubber. Increasing the flow rate from 2.5 to 10 CMM reduced the denitrification efficiency from 100 to 93.90%. Therefore, low inlet flow rates are recommended. If increasing the inlet flue gas flow rate is necessary in practical operations, the droplet size should be increased to maintain a stable droplet flow.

(3) Increasing the L/G ratio in the scrubber can increase the gas−liquid contact area, increasing the flue gas absorption efficiency of the droplets. For instance, increasing the L/G ratio from 12 to 16 L/m^3 increased the desulfurization and denitrification efficiencies slightly from 99.90 to 99.98% and from 99.76 to 99.80%, respectively.

(4) Optimizing the nozzle design can enhance spray dispersion, enhancing the gas−liquid contact. In particular, compared with other types of nozzles, a swirl cone nozzle can provide a wider spray pattern, leading to a larger gas−liquid contact area. The desulfurization and denitrification efficiencies were increased to 99.99% and 99.81%, respectively, exceeding those for full and hollow-cone nozzles.

These findings contribute to a deeper understanding of the factors influencing simultaneous desulfurization and denitrification in multistage wet scrubbers and provide valuable reference and guidance for the future design and operation of industrial-scale spray scrubbers.

AUTHOR INFORMATION

Corresponding Author

Chung-Hwan Jeon − *School of Mechanical Engineering, Pusan National University, Busan 46241, Republic of Korea; Pusan Clean Energy Research Institute, Pusan National University, Busan 46241, Republic of Korea;* orcid.org/0000-0001-8186-3323; Phone: +82-51-510-3051; Email: chjeon@pusan.ac.kr; Fax: +82-51-510-5236

Authors

Yijie Zeng − *School of Mechanical Engineering, Pusan National University, Busan 46241, Republic of Korea*

Byoung-Hwa Lee − *Pusan Clean Energy Research Institute, Pusan National University, Busan 46241, Republic of Korea*

Kang-Min Kim − *Korea Electric Power Research Institute, Daejeon 34056, Republic of Korea*

Min-Woo Kim − *School of Mechanical Engineering, Pusan National University, Busan 46241, Republic of Korea*

Young-Joo Lee − *Korea Institute of Energy Research, Daejeon 34129, Republic of Korea*

Young-Chan Choi − *Korea Institute of Energy Research, Daejeon 34129, Republic of Korea;* orcid.org/0000-0002-6111-5579

Jong Won Choi − *Korea Institute of Energy Research, Daejeon 34129, Republic of Korea*

Complete contact information is available at: https://pubs.acs.org/10.1021/acsomega.3c10223

Notes

The authors declare no competing financial interest.

https://doi.org/10.1021/acsomega.3c10223
ACS Omega 2024, 9, 15372−15382

■ ACKNOWLEDGMENTS

This work was supported by the Korea Environment Industry and Technology Institute (KEITI) through the Reduction Management Program of Fine Dust Blind Spots funded by the Korea Ministry of Environment (MOE) (number 2020003060005), the National Research Foundation of Korea, and the Ministry of Science, ICT, and Future Planning (grant number 2022K1A4A8A01080312).

■ NOMENCLATURE

A_d surface area of the droplet, m^2
C_l gas concentration in the droplets
C_d drag coefficient
D_{H_2O} diffusion coefficients in the liquid phase, m^2/s
D_{N_2} diffusion coefficients in the gas phase, m^2/s
d_p diameter of droplet, mm
E enhancement factor
H Henry's constant, Pa m^3 $kmol^{-1}$
J absorption rate, kmol m^{-2} s^{-1} Pa^{-1}
K_{tot} overall mass transfer coefficient, kmol m^{-2} s^{-1} Pa^{-1}
k_l mass transfer coefficient in the liquid phase, kmol m^{-2} s^{-1} Pa^{-1}
k_g mass transfer coefficient in the gas phase, kmol m^{-2} s^{-1} Pa^{-1}
m mass, kg
P pressure, Pa
Re Reynold number
R the universal gas constant, 8.314 J/(mol·K)
Sc the Schmidt number
S source term
T temperature, K
$\vec{u}$ velocity, m/s

■ GREEK LETTERS

ρ density, kg/m^3
σ surface tension of the droplet, N m^{-1}

■ SUBSCRIPTS

d droplet
g gas phase
k gas species
l liquid phase

■ ABBREVIATIONS

SCR, selective catalytic reduction; FGD, flue gas desulfurization; WFGD, wet flue gas desulfurization; UDF, user-defined function; L/G, liquid-to-gas

■ REFERENCES

(1) Clark, N. A.; Demers, P. A.; Karr, C. J.; Koehoorn, M.; Lencar, C.; Tamburic, L.; Brauer, M. Effect of early life exposure to air pollution on development of childhood asthma. *Environ. Health Perspect.* **2010**, *118* (2), 284−290.
(2) Kerr, H. D.; Kulle, T. J.; McIlhany, M. L.; Swidersky, P. Effects of nitrogen dioxide on pulmonary function in human subjects: an environmental chamber study. *Environ. Res.* **1979**, *19* (2), 392−404.
(3) Sims, J. N.; Leggett, S. S.; Myla, A. Industrial emissions and asthma prevalence. *Eur. J. Environ. Publ. Health* **2020**, *4* (2), No. em0046.
(4) Liu, Y.; Wang, Z.; Ke, W. Study on influence of native oxide and corrosion products on atmospheric corrosion of pure Al. *Corros. Sci.* **2014**, *80*, 169−176.
(5) Chen, D.; Zhang, Z.; Li, Z.; Lv, Z.; Cai, N. Optimizing in-situ char gasification kinetics in reduction zone of pulverized coal air-staged combustion. *Combust. Flame* **2018**, *194*, 52−71.
(6) Jiang, Y.; Lee, B. H.; Oh, D. H.; Jeon, C. H. Optimization of operating conditions to achieve combustion stability and reduce NOx emission at half-load for a 550-MW tangentially fired pulverized coal boiler. *Fuel* **2021**, *306*, 121727.
(7) Wang, H.; Yuan, B.; Hao, R. L.; Zhao, Y.; Wang, X. P. A critical review on the method of simultaneous removal of multi-air-pollutant in flue gas. *Chem. Eng. J.* **2019**, *378*, 122155.
(8) Cheng, X.; Bi, X. T. A review of recent advances in selective catalytic NOx reduction reactor technologies. *Particuology* **2014**, *16*, 1−18.
(9) Abdulrasheed, A. A.; Jalil, A. A.; Triwahyono, S.; Zaini, M. A. A.; Gambo, Y.; Ibrahim, M. Surface modification of activated carbon for adsorption of SO_2 and NO_X: a review of existing and emerging technologies. *Renewable Sustainable Energy Rev.* **2018**, *94*, 1067−1085.
(10) Sharif, H. M. A.; Mahmood, N.; Wang, S. Y.; Hussain, I.; Hou, Y. N.; Yang, L. H.; Zhao, X.; Yang, B. Recent advances in hybrid wet scrubbing techniques for NOx and SO_2 removal: State of the art and future research. *Chemosphere* **2021**, *273*, 129695.
(11) Zhao, M. J.; Xue, P.; Liu, J. J.; Liao, J. H.; Guo, J. M. A review of removing SO_2 and NOx by wet scrubbing. *Sustain. Energy Technol. Assessments* **2021**, *47*, 101451.
(12) Magli, F.; Capra, F.; Gatti, M.; Martelli, E. Process selection, modelling and optimization of a water scrubbing process for energy-self-sufficient biogas upgrading plants. *Sustain. Energy Technol. Assessments* **2018**, *27*, 63−73.
(13) Chmielewski, A. G.; Han, B. S. Electron Beam Technology for Environmental Pollution Control. *Top. Curr. Chem.* **2016**, *374*, 68.
(14) Pawelec, A.; Chmielewski, A. G.; Sun, Y. X.; Bułka, S.; Torims, T.; Pikurs, G.; Mattausch, G. Plasma technology to remove NOx from off-gases. *Nukleonika* **2021**, *66*, 227−231.
(15) Wang, S.; Fan, Q.; Xu, S.; Gao, S.; Xiao, P.; Jiang, M. Simultaneous removal of SO2 and NOx from flue gas by low-temperature adsorption over activated carbon. *Sci Rep.* **2020**, *11*, 11003.
(16) Zhao, Z. Y.; Zhang, Y. X.; Gao, W. C.; Baleta, J.; Liu, C.; Li, W. J.; Weng, W. G.; Dai, H. B.; Zheng, C. H.; Gao, X. Simulation of SO_2 absorption and performance enhancement of wet flue gas desulfurization system. *Process Saf. Environ. Prot.* **2021**, *150*, 453−463.
(17) Qu, J. Y.; Qi, N. N.; Zhang, K.; Li, L. F.; Wang, P. C. Wet flue gas desulfurization performance of 330-MW coal-fired power unit based on computational fluid dynamics region identification of flow pattern and transfer process. *Chin. J. Chem. Eng.* **2021**, *29*, 13−26.
(18) Chen, J.; Chen, Y.; Hrynsphan, D.; Mei, Y.; Pan, H.; Wu, J. L.; Chen, J. M.; Yao, J. C. FeII, Fe II (EDTA)-NO reduction by Mn powder in wet flue gas denitrification technology coupled with Mn^{2+} recycling: Performance, kinetics, and mechanism. *Energy Fuels* **2020**, *34*, 2590−2598.
(19) Qu, J. Y.; Qi, N. N.; Li, Z.; Zhang, K.; Wang, P. C.; Li, L. F. Mass transfer process intensification for SO_2 absorption in a commercial-scale wet flue gas desulfurization scrubber. *Chem. Eng. Process.* **2021**, *166*, 108478.
(20) Chen, Z.; Wang, H. M.; Zhuo, J. K.; You, C. F. Experimental and numerical study on effects of deflectors on flow field distribution and desulfurization efficiency in spray towers. *Fuel Process. Technol.* **2017**, *162*, 1−12.
(21) Kurella, S.; Bhukya, P. K.; Meikap, B. C. Removal of H_2S pollutant from gasifier syngas by a multistage dual-flow sieve plate column wet scrubber. *J. Environ. Sci. Health, Part A: Toxic/Hazard. Subst. Environ. Eng.* **2017**, *52*, 515−523.
(22) Swamy, K.; Meikap, B. C. Hydrodynamic characteristics of a three-stage dual-flow sieve plate scrubber. *S. Afr. J. Chem. Eng.* **2017**, *23*, 91−97.
(23) Tran, T. V.; Narabayashi, T.; Takahashi, H.; Kikura, H. Effects of the baffle plate of the advanced Venturi scrubber on decontamination factor of the filtered containment venting system. *Jpn. J. Multiphas. Flow* **2021**, *35*, 337−345.

https://doi.org/10.1021/acsomega.3c10223
ACS Omega 2024, 9, 15372−15382

(24) Tseng, C. C.; Li, C. J. Numerical investigation of the inertial loss coefficient and the porous media model for the flow through the perforated sieve tray. *Chem. Eng. Res. Des.* **2016**, *106*, 126−140.
(25) Tseng, C. C.; Li, C. J. Eulerian-Eulerian numerical simulation for a flue gas desulfurization tower with perforated sieve trays. *Int. J. Heat Mass Transfer* **2018**, *116*, 329−345.
(26) Zhuang, Z. K.; Sun, C. L.; Zhao, N.; Wang, H. Q.; Wu, Z. B. Numerical simulation of NO_2 absorption using sodium sulfite in a spray scrubber. *J. Chem. Technol. Biotechnol.* **2016**, *91*, 994−1003.
(27) Li, X.; Dong, M. R.; Li, S. D.; Feng, Z. Y.; Zhang, Z. P.; Li, W. J.; Ren, Y. J.; Lu, J. D. A numerical study of the ammonia desulfurization in the spray scattering scrubber. *Chem. Eng. Process.* **2020**, *155*, 108069.
(28) Gómez, A.; Fueyo, N.; Tomás, A. Detailed modelling of a flue-gas desulfurization plant. *Comput. Chem. Eng.* **2007**, *31*, 1419−1431.
(29) Crowe, C. T.; Schwarzkopf, J. D.; Sommerfeld, M. *Multiphase Flows with Droplets and Particles*; CRC Press, 2012.
(30) Qin, M. C.; Dong, Y.; Cui, L.; Yao, J. W.; Ma, C. Y. Pilot-scale experiment and simulation optimization of dual-loop wet flue gas desulfurization spray scrubbers. *Chem. Eng. Res. Des.* **2019**, *148*, 280−290.
(31) Morsi, S. A.; Alexander, A. J. An investigation of particle trajectories in two-phase flow systems. *J. Fluid Mech.* **1972**, *55*, 193−208.
(32) Levenspiel, O. *Chemical Reaction Engineering*; Wiley: New York, 1999.
(33) Neveux, T.; Le Moullec, Y. Wet industrial flue gas desulfurization unit: Model development and validation on industrial data. *Ind. Eng. Chem. Res.* **2011**, *50*, 7579−7592.
(34) Dou, B.; Pan, W.; Jin, Q.; Wang, W.; Li, Y. Prediction of SO2 removal efficiency for wet Flue Gas Desulfurization. *Energy Convers. Manage.* **2009**, *50* (10), 2547−2553.
(35) He, F. Q.; Zhu, X. Y.; Chen, X. C.; Ding, J. H. Performance, mechanism, and kinetics of NO removal by combined ascorbic acid and Fe(II)(EDTA) reaction systems. *Fuel* **2021**, *284*, 119070.
(36) Sada, E.; Kumazawa, H.; Kudo, I.; Kondo, T. Individual and simultaneous absorption of dilute NO and SO_2 in aqueous slurries of $MgSO_3$ with FeII-EDTA. *Ind. Eng. Chem. Process Des. Dev.* **1980**, *19* (3), 377−382.
(37) Wankat, P. C. *Equilibrium Staged Separations*; Prentice Hall: NJ, 1988.
(38) Wang, P. H.; Dai, G. Synergistic effect between spraying layers on the performance of the WFGD spray column. *Asia-Pac. J. Chem. Eng.* **2018**, *13*, 2266.
(39) Wu, X.; Zhao, H.; Zhang, Y.; Zheng, C.; Gao, X. Measurement of slurry droplets in coal-fired flue gas after WFGD. *Environ. Geochem. Health* **2015**, *37*, 915−929.
(40) Chu, G. W.; Fei, J.; Cai, Y.; Liu, Y. Z.; Gao, Y.; Luo, Y.; Chen, J. F. Removal of SO_2 with sodium sulfite solution in a rotating packed bed. *Ind. Eng. Chem. Res.* **2018**, *57*, 2329−2335.
(41) Han, J.; Yao, X.; Qin, L. B.; Jiang, M.; Xing, F. T.; Chen, W. S. Simultaneous removing SO_2 and NO by ammonia-FeII EDTA solution coupled with iron regeneration. *Int. J. Environ. Res.* **2016**, *10*, 519−524.
(42) Zhou, J. X.; Wang, H. W. Study on efficient removal of SOx and NOx from marine exhaust gas by wet scrubbing method using urea peroxide solution. *Chem. Eng. J.* **2020**, *390*, 124567.

https://doi.org/10.1021/acsomega.3c10223
ACS Omega 2024, 9, 15372−15382